TESTING AND ANALYSIS CORRELATION OF COMPOSITE SANDWICH LONGITUDINAL BONDED JOINTS FOR SPACE LAUNCH VEHICLE STRUCTURES

David W. Sleight, Arunkumar Satyanarayana, Brian H. Mason
NASA Langley Research Center, Hampton, VA 23681, USA

Babak Farrokh, and Kenneth Segal
NASA Goddard Space Flight Center, Greenbelt, MD 20771, USA

ABSTRACT

The NASA Composite Technology for Exploration (CTE) Project has been developing and demonstrating critical composite technologies with a focus on joints; incorporating materials, design/analysis, manufacturing, and tests that utilize NASA expertise and capabilities. The CTE project has focused on the development of composite longitudinal bonded joint technologies for conical structures such as the SLS Payload Attach Fitting (PAF) due to challenging joint geometries and loads compared to cylindrical jointed structures. The CTE team selected and designed a double-lap composite bonded joint as the most advantageous longitudinal joint to advance for the CTE project. This paper reports on the longitudinal bonded joint sub-element test articles that were fabricated and tested for several loading conditions to test the capability of the bonded joint design. Test and analysis correlation to the sub-element test articles are presented in the paper.

1. INTRODUCTION

The NASA Composite Technology for Exploration (CTE) Project has been developing and demonstrating critical composite technologies with a focus on joints; incorporating materials, design/analysis, manufacturing, and tests that utilize NASA expertise and capabilities. The CTE project kicked off in 2017 and is a multi-Center project led by Marshall Space Flight Center (MSFC) and supported by Glenn Research Center (GRC), Goddard Space Flight Center (GSFC), Kennedy Space Center (KSC), and the Langley Research Center (LaRC). The project has been funded by the Game Changing Development (GCD) Program in the Space Technology Mission Directorate (STMD) and the Spacecraft Payload Integration and Evolution (SPIE) Office in the Space Launch System (SLS) Program. The project has goals of advancing composite technologies and providing lightweight structures to support future NASA exploration missions. In particular, the CTE project has plans to demonstrate weight-saving, performance-enhancing composite bonded joint technology for Space Launch System (SLS)-scale composite hardware. Advancements from the CTE project may be incorporated as future block upgrades for SLS structural components. Further, the project will advance the state of the art in the detailed analyses of composite bonded joints for joint failure prediction. The CTE project builds upon composite design and manufacturing knowledge obtained from earlier NASA programs [1-5].

For the first two years of the project, the CTE project focused on the development of composite longitudinal bonded joint technologies for conical structures such as the SLS Payload Attach Fitting (PAF) due to challenging joint geometries and loads compared to cylindrical jointed structures. As shown in Figure 1, the conical PAF resides within the Universal Stage Adapter (USA) in the Exploration Upper Stage (EUS) of the SLS. Payloads for the SLS are mounted atop the PAF. Alternative SLS configurations also allow for payload only missions with a fairing instead of the USA. The diameter of the conical PAF at its bottom circumferential joint is 8.4 meters, making the PAF too large to manufacture as one piece in all but the largest autoclaves; therefore, the PAF is being designed to be manufactured in eight sections connected with longitudinal joints (see Figure 1). As part of this focus on longitudinal bonded joint technologies for conical structures, the CTE project worked with the SLS/PAF team to develop a generic PAF design called the *CTE Point Design* with a goal of advancing manufacturing and analysis prediction technologies for composite longitudinal bonded joints. A description of this development effort for the longitudinal bonded joint is included in reference [6].

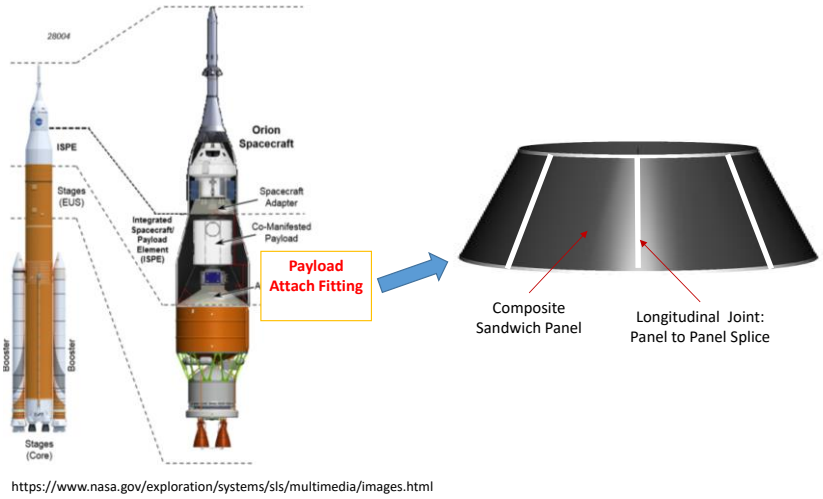

https://www.nasa.gov/exploration/systems/sls/multimedia/images.html

Figure 1. Exploded view of SLS showing PAF.

The focus of this proposed paper will be on the sub-element joint testing and analysis correlation for the CTE project. This paper is organized as follows. Section II provides a brief description of the structural design of a composite longitudinal bonded joint and the sub-element joint test coupons. Section III presents a description of the sub-element joint testing for various loading conditions and includes a summary of the test results and test/analysis correlation for pre-test and post-test predictions. A description of the analysis methodology is also presented. Finally, a summary of the effort is presented in Section IV.

2. CTE LONGITUDINAL BONDED JOINT AND SUB-ELEMENT TEST COUPON DESIGN

The CTE project leveraged joint trade studies for longitudinal joints from past NASA projects, the Advanced Composite Technology (ACT) Project which ran from 2008-2010, the Lightweight Spacecraft Structures & Materials (LSSM) Project which ran from 2010-2011, and the Composites for Exploration Upper State (CEUS) project which ran from 2014-2016. A double-lap composite bonded joint was selected as the most advantageous longitudinal joint to advance for the CTE

project. The joint selection was based on an assessment of figures of merit for mass, damage tolerance, inspectability, cost, design/analysis uncertainty, and producability. The *CTE Point Design* as shown in Figure 2, is a conical sandwich structure with a 35-degree angle consisting of eight composite sandwich segments joined together with a double lap composite joint. The down-selected composite double lap bonded joint joins the segmented composite sandwich panel sections together by bonding a prepreg fabric doubler using FM209-1M adhesive. The sections were affixed adjacent to one another with a 2.54 mm gap between them and filled with EA9396.6MD. The acreage panels chosen were a sandwich construction with a 25.4 mm Plascore 49.66 kg/m^3 aluminum core (5056) with 4.76 mm hexagonal cells and IM7/8552-1 quasi-isotropic graphite/epoxy face sheets. The doubler material used was 5320-1/PW T650 3K epoxy and carbon fiber woven prepreg from Solvay Industries.

Longitudinal jointed flat panels were manufactured based on the design described above and then manufactured into longitudinal joint sub-element test articles for several configurations to test various critical loading conditions of the *CTE Point Design*. The sub-element joint configurations included Axial Edge-Wise Compression (AEWC), Hoop Edge-Wise Compression (HEWC), and Hoop Edge-Wise Tension (HEWT) coupons. Their design details are presented below.

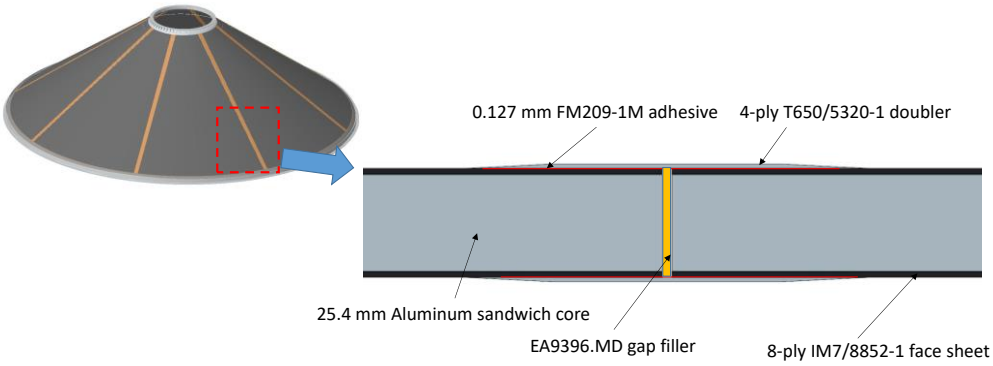

Figure 2. *CTE Point Design* Joint.

2.1 Axial Edge-Wise Compression (AEWC) Coupons

The AEWC coupons were sized to be 198.1 mm long by 157.5 mm wide as shown in Figure 3 (a). In preparation for testing, the load introduction ends of the bonded segments were designed to be potted in order to better stabilize the face sheets and to prevent local crushing. The load introduction ends consisted of aluminum frames to contain the potting material and to provide additional lateral support during handling and testing. Edge relief was included by removing some of the potting material around the edges of the test article to alleviate high stress concentrations of the core. The design of the AEWC coupons was sized by linear static and buckling analysis with Nx Nastran [7]. The goal was to design the AEWC sub-element coupons to fail at the joint location; however, multiple analysis iterations were unable to find a coupon design that would fail at the joint.

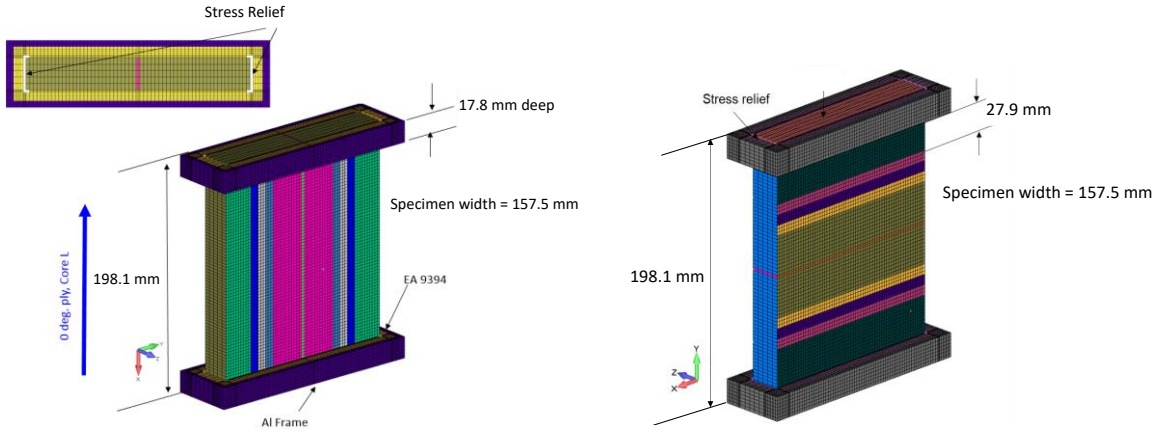

(a.) AEWC Coupon (b.) HEWC Coupon

Figure 3. AEWC and HEWC Coupon Size and Geometry (with Potted Ends).

2.2 Hoop Edge-Wise Compression (HEWC) Coupons

The HEWC sub-element coupons were the same size (198.1 mm long by 157.5 mm wide) as the AEWC sub-element coupons as shown in Figure 3 (b). In preparation for testing, the load introduction ends of the bonded segments were designed to be potted in order to better stabilize the face sheets and to prevent local crushing. The load introduction ends consisted of aluminum frames to contain the potting material and to provide additional lateral support during handling and testing. The design of the HEWC coupons was sized by linear static and buckling analysis with Nx Nastran. The HEWC coupons were designed to fail at the joint location according to preliminary analysis.

2.3 Hoop Edge-Wise Tension (HEWT) Coupons

The HEWT test specimens were designed to have dimensions of 558.8 mm by 76.2 mm as shown in Figure 4. The core at the load introduction ends of the specimens was removed to a depth of 86.4 mm. and an aluminum insert which was 25.4 mm thick at the core and tapered to 15.2 mm at the free end was inserted at either end of the panel and attached to the face sheet with adhesive. The test specimens were designed to fail at the joint location.

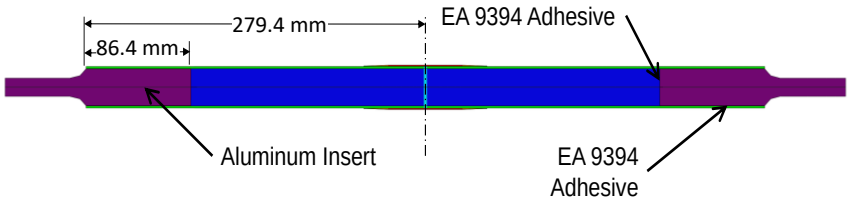

Figure 4. HEWT Coupon Size and Geometry (with Aluminum Inserts).

3. LONGITUDINAL JOINT SUB-ELEMENT TESTING AND ANALYSIS CORRELATION

In order to assess the structural performance of the CTE longitudinal composite sandwich bonded joint design and to validate the structural models for joint failure prediction, the CTE team devised an extensive test matrix determined by the structural analysis effort for various critical loading conditions based on the longitudinal joint. These loading conditions included axial compression, hoop compression, and hoop tension applied loadings. Multiple replicates of sub-element jointed test coupons were machined from the composite sandwich bonded jointed panels and tested for failure both in pristine conditions and damage conditions with impact-damage at the center of the joint at Southern Research in Birmingham, AL. The next sections include a summary of the pristine test results for the AEWC, HEWC, and HEWT joint sub-element specimen testing conducted at SR from May-July 2018. Progressive failure analyses (PFA) and cohesive zone modeling (CZM) were used to predict the joint failure load and location for each joint coupon test. A description of the PFA used to predict the failure of the sub-element specimen testing is presented. Lastly, correlation with pre-test and post-test analysis predictions with the test results are discussed.

3.1 Progressive Failure Analysis Methodology

The progressive failure analysis procedure adopted in this work to evaluate strength and failure mode of longitudinal joint coupons consists of three steps. The first step in failure analysis is to determine damage at the material point. This was accomplished by adopting Hashin-Rotem failure criteria.

Fiber Damage: *Tension & compression*

$$\left(\frac{\sigma_{11}}{X_T}\right) \geq 1 \; for \; \sigma_{11} \geq 0 \, , df = 0.8 \qquad \left(\frac{\sigma_{11}}{X_C}\right) \geq 1 \; for \; \sigma_{11} < 0 \, , df = 0.8$$

Matrix Damage: *Tension , compression & Shear*

$$\left(\frac{\sigma_{22}}{Y_T}\right)^2 + \left(\frac{\sigma_{12}}{S_{12}}\right)^2 \geq 1 \; for \; \sigma_{22} \geq 0 \, , dM = 1.0 \qquad \left(\frac{\sigma_{22}}{Y_C}\right)^2 + \left(\frac{\sigma_{12}}{S_{12}}\right)^2 \geq 1 \; for \; \sigma_{22} \leq 0 \, , dM = 1.0$$

σ_{11} = Stress in 1 (fiber) direction
σ_{22} = Stress in 2 (transverse) direction
σ_{12} = In-plane shear stress
ε_{11} = Strain in 1 (fiber) direction
ε_{22} = Strain in 2 (transverse) direction
ε_{12} = In-plane shear strain

X_T = Tensile failure stress of fiber
X_C = Compressive failure stress of fiber
Y_T = Tensile failure stress of matrix
Y_C = Compressive failure stress of matrix
S_{12} = shear strength of matrix

[1]

The failure indices d_f & d_m represent damage status of fiber and matrix material system. Damage index d_f will be zero up until failure and attains a value of 0.8 upon failure. However the damage index d_m will be zero up until failure and attains a value of 1.0 upon failure. The Hooke's law along with failure indices is presented below.

$$\begin{pmatrix}\sigma_{11}\\ \sigma_{22}\\ \sigma_{12}\end{pmatrix} = \begin{pmatrix}(1-df)\,Q_{11} & (1-df)(1-dm)\,Q_{12} & 0\\ (1-df)(1-dm)\,Q_{12} & (1-df)(1-dm)\,Q_{22} & 0\\ 0 & 0 & (1-df)(1-dm)\,Q_{66}\end{pmatrix}\begin{pmatrix}\varepsilon_{11}\\ \varepsilon_{22}\\ \varepsilon_{12}\end{pmatrix}$$

$Q_{11} = E_{11} / \Delta$
$Q_{22} = E_{22} / \Delta$
$Q_{12} = \nu_{12} E_{22} / \Delta$
$Q_{66} = G_{12} / \Delta$
$\Delta = 1 - \nu_{12}\nu_{12}(1 - d_M)$

E_{11} = Elastic Modulus in 1 (fiber) direction
E_{22} = Elastic Modulus in 2 (transverse) direction
G_{12} = In-plane Shear Elastic
ν_{12} = Poisson's ratio

[2]

Once a material point reaches the failure limit, the stresses are degraded as show in Figure 5 below. The area under the stress-strain curve equates to the fracture energy of fiber (G_{Fc}) and matrix (G_{Mc}) of the material system. The strain scale factor N determines the ultimate strain that equates to the fiber fracture energy toughness. Failed elements were removed from the model to simulate virtual crack growth when in-plane strain reaches a value of 0.25.

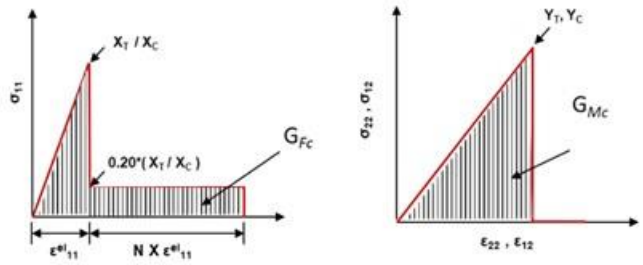

Figure 5. Stress Degradation Profiles for Damage Simulation.

The failure load provided by this damage model is independent of finite element size as long as the edges are within 0.254 mm to 4.06 mm length. Additional information on mesh regularization procedure and its validation is presented in reference [8].

3.2 Axial Edge-Wise Compression (AEWC) Coupons

The test stand & compression test setup for both pristine and impacted AEWC coupons is shown in 6. The coupon is placed between a flat square platen at the bottom and a thick rectangular steel block, covering the entire width and thickness of the coupon, on the top. Above the thick steel block, a circular cross-section steel block is placed. The AEWC sub-element coupons were instrumented with strain gages and a digital image correlation (DIC) system to obtain full field, displacement and strain contours. The joint testing included 10 pristine AEWC sub-element test coupons.

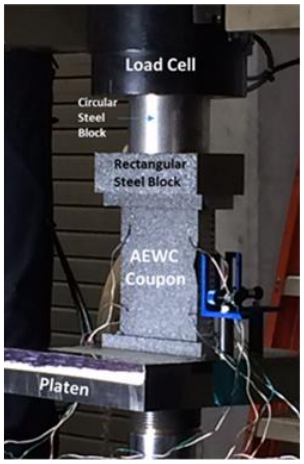

Figure 6. Test Setup & Strain Gauge Configuration of AEWC Coupon.

3.2.1 Progressive Failure Analysis of Pristine Coupon

Progressive failure analysis of the AEWC coupons was performed by adopting the damage model mentioned in the previous section. This model is capable of simulating fiber and matrix damages using 2-D stress state. Upon a closer examination of the loading and geometric configuration of this coupon, it was inferred that delamination between plies or any sub-assemblies was not an issue and hence the finite element model was developed to simulate only fiber and matrix damages. The post-test finite element model is presented in Figure 7 showing various components of the joint and boundary conditions. The frames at the ends of the coupon were not modeled explicitly but the influence of it was simulated by appropriately constraining the nodes. Pre- test and post-test finite element models as essentially the same except that the fiber compression modulus was used in the post-test analysis and stress release length in the model was increased by un-constraining nodes in the frame region. The general-purpose finite-element code, Abaqus Standard 6.13 [9], was used to perform the finite-element analysis (FEA). Solid elements (C3D8) were used to discretize core, adhesive and gap filler regions. The face sheet and splice plate were discretized using shell continuum (SC8R) elements.

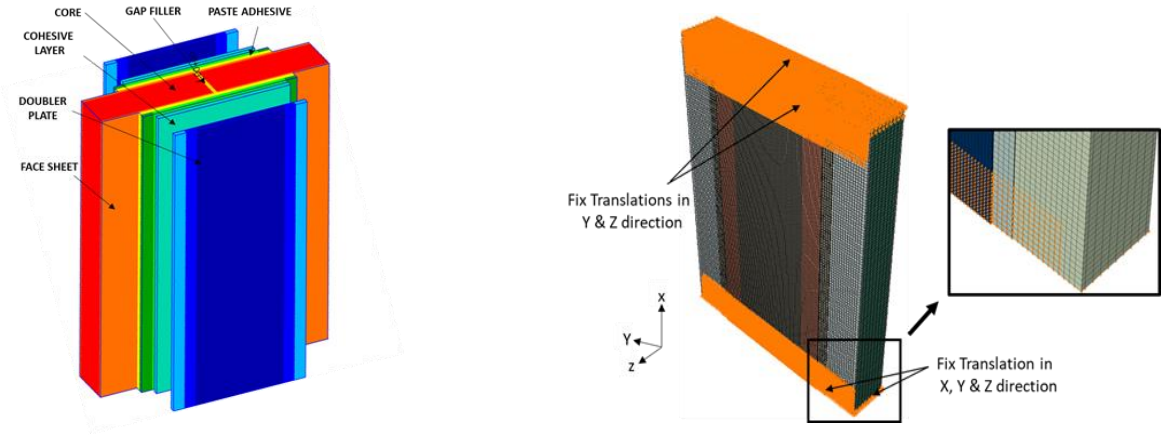

(a) Modeling Details of AEWC Coupon. (b) Actual FEM & Simulation of Boundary Condition without End Fixtures

Figure 7. Finite Element Model Description of AEWC Coupon.

3.2.2 Pristine Coupon Testing & PFA Correlation

Ten pristine coupons were tested and the average failure load was 179.938 kN as listed in Table 1. The failure mode of these coupons were in the form of fiber failure in the face sheet at grips and delamination between face sheet plies which is an after effect of earlier failure mode. Pre-test and post-test progressive failure analysis (PFA) generated the failure load of 195.722 kN and 185.935 kN, which is 8.8 % and 3.3 % respectively from the test failure load and load vs. end shortening curves are presented in Figure 8. The failure modes (fiber failure at the grips)of the test coupons and the failure modes simulated by PFA are presented in Figure 9. One can notice a good agreement between the test and PFA with respect to location of failure initiation and the path. The crack paths are indicated by red color in the PFA model.

Table 1. Test Data of AEWC Coupons.

AEWC Specimen ID	Test Failure Load (kN)
CTE-301-3-AEWC - 1	179.877
CTE-301-3-AEWC - 3	188.084
CTE-301-3-AEWC - 4	171.666
CTE-301-3-AEWC - 5	177.871
CTE-301-4-AEWC - 1	172.542
CTE-301-4-AEWC - 2	188.124
CTE-301-4-AEWC - 3	179.806
CTE-301-4-AEWC - 4	181.078
CTE-301-4-AEWC - 5	180.398
Average	**179.938**

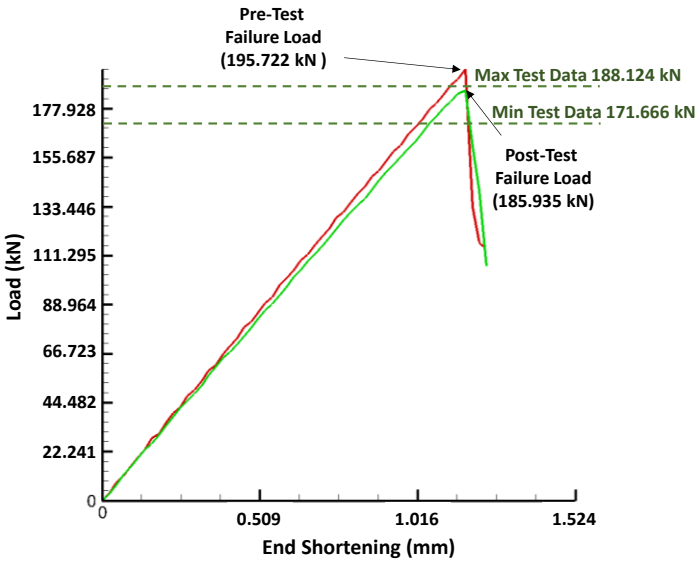

Figure 8. Load vs. End Shortening of AEWC PFA.

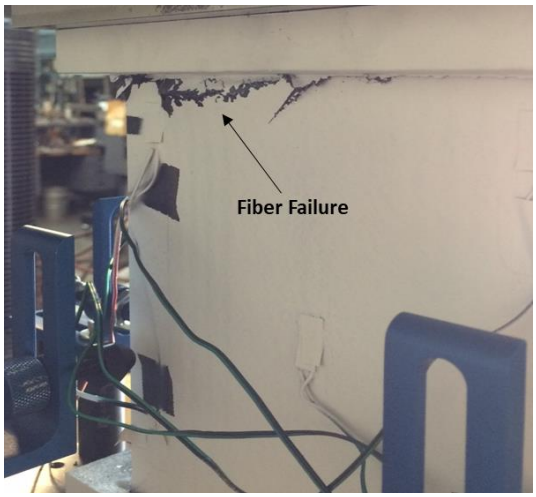

(a) Typical Failure Mode of AEWC Coupon

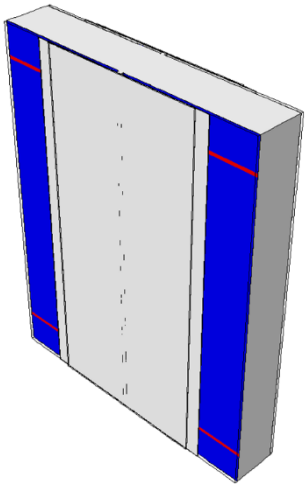

(b) Failure Mode Predictions from PFA

Figure 9. Typical Failure Mode of AEWC Coupon.

3.3 Hoop Edge-Wise Compression (HEWC) Coupons

The test stand and compression test setup for both pristine and impacted HEWC coupons is the same as in the AEWC test shown previously in Figure 6. The coupon is placed between a flat square platen at the bottom, and a thick rectangular steel block, covering the entire width and thickness of the coupon, on the top. A circular cross-section steel block is placed above the thick steel block. The joint testing included 7 pristine HEWC sub-element test coupons.

3.3.1 Progressive Failure Analysis of Pristine Coupon

Progressive failure analysis of HEWC was performed by adopting the damage model mentioned in sub-section A for predicting in-plane failure modes such as fiber and matrix damages. After closer examination of loading and geometric configuration of the coupon, it was inferred that delamination between plies or any sub-assemblies would be primary mode of failure. Hence, the finite element model was developed to simulate fiber and matrix damages in the face sheet plies as well as delamination between face sheet plies and splice (doubler) plate plies. The finite element model is presented in Figure 10 showing various components of the joint and boundary conditions. The frames at the ends of the coupon were not modeled explicitly but the influence of it was simulated by appropriately constraining the nodes. Delamination damage mode is simulated with the help of built-in cohesive zone model (CZM) in Abaqus. Solid elements (C3D8) were used to discretize core, adhesive and gap filler regions. The face sheet and splice plate were discretized using shell continuum (SC8R) elements and the cohesive layers are discretized using COH3D8 elements.

3.3.2 Pristine Coupon Testing & PFA Correlation

Seven pristine coupons were tested and the average failure load was 95.30 kN as listed in Table 2. The failure mode of these coupons were in the form delamination between the outer face sheet ply and the adjacent ply, close to the adhesive layer. Some fiber failure was noticed in outer face sheet

plies at the termination point of splice plates. Progressive failure analysis (PFA) generated a max failure load of 92.43 kN, which is within 3.0 % of test failure load. Load vs. end shortening curves are presented in Figure 11. One can notice in this figure, that the delamination grew gradually starting from 87.41 kN. Delamination plots as a function of load are also presented in Figure 11. The typical failure mode (delamination between the face sheet plies) of the test coupons and the modes simulated by PFA are in excellent agreement as can be noticed in Figure 12.

Table 2. Test Data of HEWC Coupons.

HEWC Specimen ID	Test Failure Load (kN)
CTE-301-5-HEWC - 1	97.95
CTE-301-5-HEWC - 2	101.20
CTE-301-5-HEWC - 3	90.92
CTE-301-9-HEWC - 1	96.75
CTE-301-9-HEWC - 2	99.20
CTE-301-10-HEWC - 1	89.14
CTE-301-10-HEWC - 2	91.94
Average	**95.30**

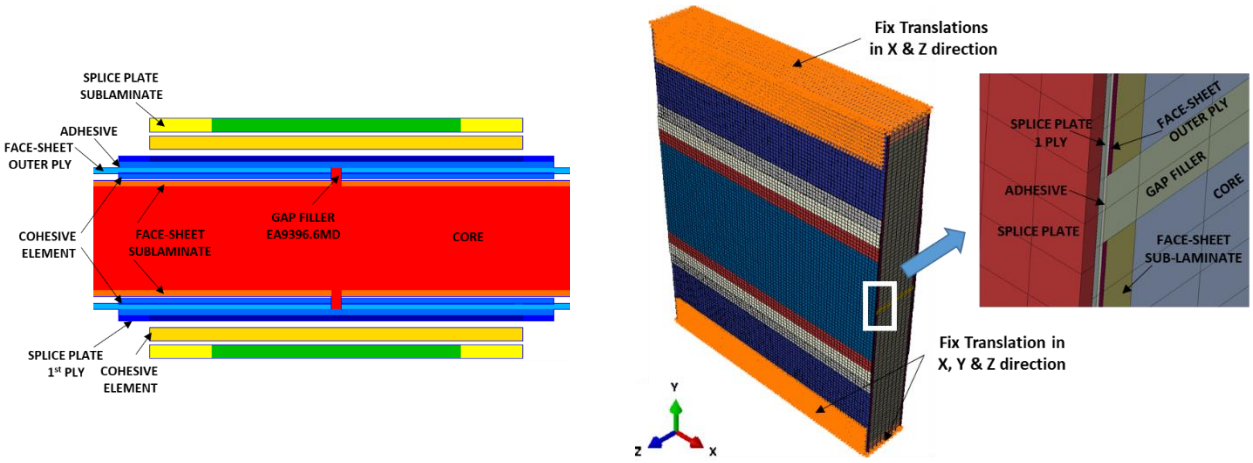

(a) Cross-Sectional View of HEWC Model (b) Actual FEM & Simulation of Boundary Condition without End Fixtures

Figure 10 Finite Element Model Description of HEWC Coupon.

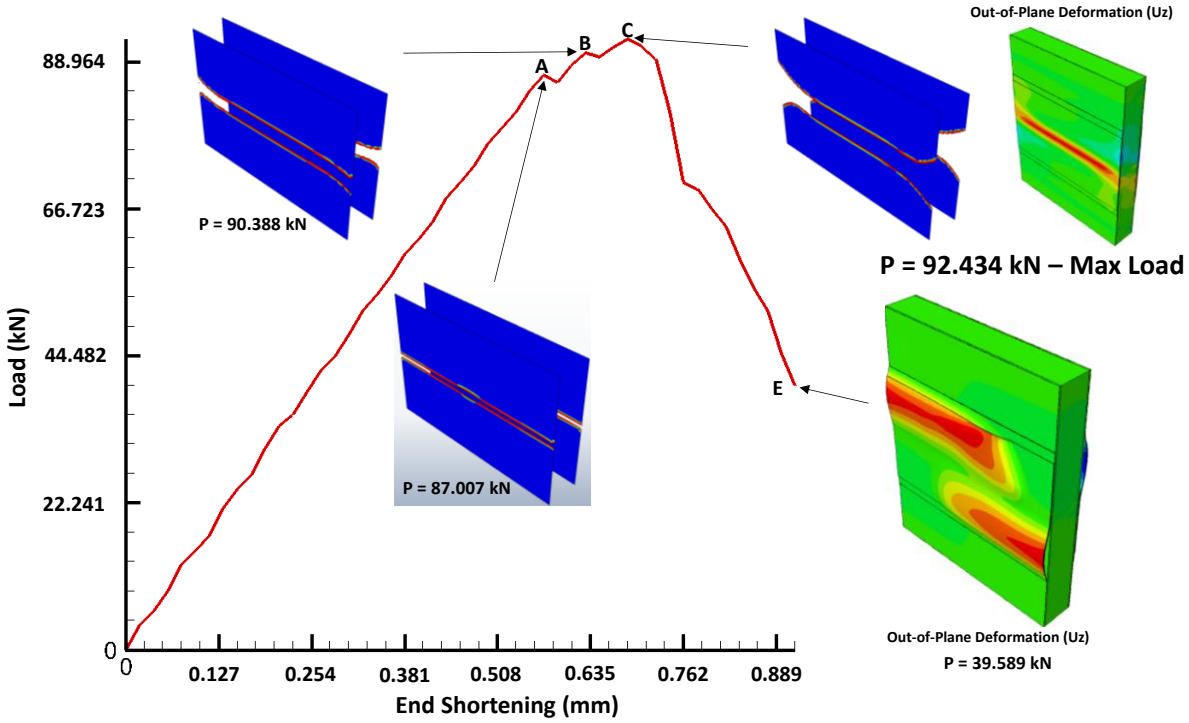

Figure 11. Load vs. End Shortening of HEWC PFA.

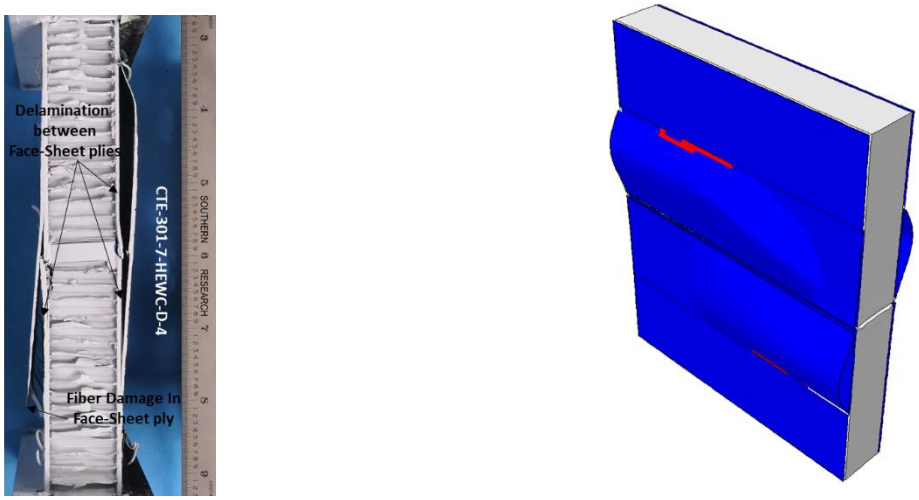

(a) Typical Failure Mode of HEWC Coupon (b) Failure Mode Predictions from PFA

Figure 12. Typical Failure mode of HEWC Coupon.

3.4 Hoop Edge-Wise Tension (HEWT) Coupons

The test stand for the HEWT coupon tests at Southern Research is shown in Figure 13. The sub-element coupons were gripped in the test machine and pulled under tension loading until failure. The joint testing included 10 pristine HEWT sub-element test coupons.

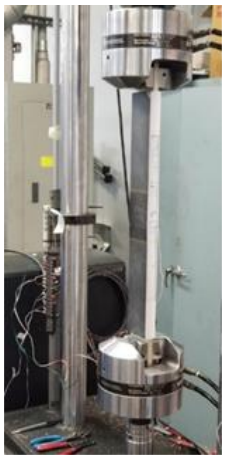

Figure 13. Test Set-up for HEWT Test at Southern Research.

3.4.1 Progressive Failure Analysis of Pristine Coupon

Progressive failure analysis of HEWT was performed by adopting the damage model mentioned in sub-section A for predicting in-plane failure modes such as fiber and matrix damages. After closer examination of loading and geometric configuration of the coupon, it was inferred that delamination between plies or any sub-assemblies would be the primary mode of failure. Hence, the finite element model was developed to simulate fiber and matrix damages in the face sheet plies as well as delamination between face sheet plies and splice (doubler) plate plies. The finite element model is presented in Figure 14 showing various components of the joint and boundary conditions. Delamination damage mode is simulated with the help of built-in cohesive zone model (CZM) in Abaqus. Solid elements (C3D8) were used to discretize core, adhesive and gap filler regions. Face sheet and splice plate were discretize using shell continuum (SC8R) elements and the cohesive layers are discretized using COH3D8 elements.

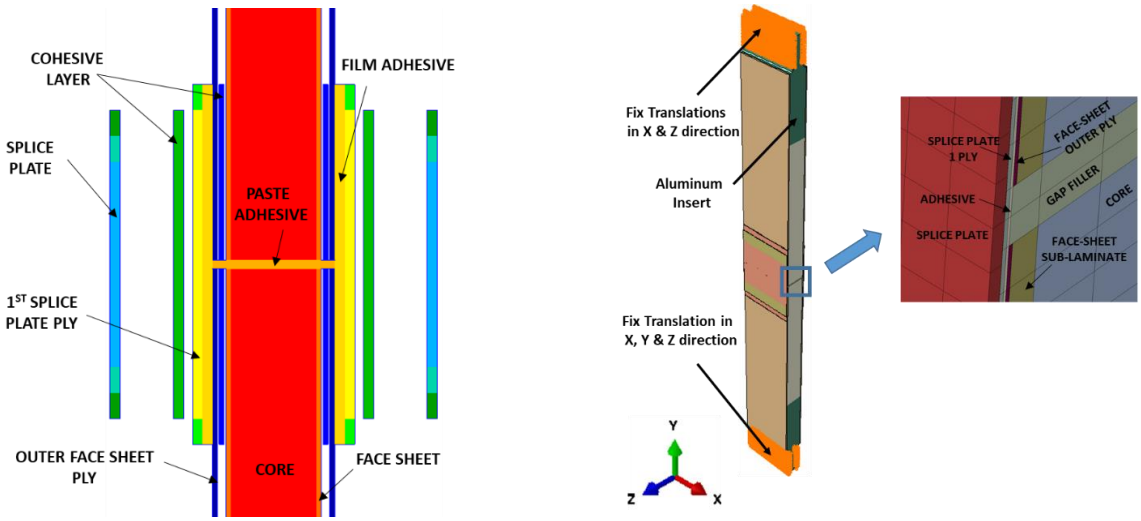

(a) Cross-Sectional View of HEWT Model

(b) Actual FEM & Simulation of Boundary Condition without End Fixtures.

Figure 14. Finite Element Model Description of HEWT Coupon.

3.4.2 Pristine Coupon Testing & PFA Correlation

Ten HEWT sub-element coupons were tested under a tensile load. Table 3 reports the failure modes and failure load of all the 10 HEWT coupons along with the axial strain at center of the joint before failure. The failure modes of the tested coupons were "Delam" (delamination between face sheet plies) and NSF (net-section failure of doubler plate). Four of the coupons failed due to "Delam" on one side and NSF on the other side. Four of the coupons failed due to NSF on both sides and two of the coupons failed due to "Delam" on both sides. The average failure load of the joint in tension is 66.785 kN. Additional information on the HT coupon testing and analysis correlation is included in reference [10]. Figure 15 presents typical the failure modes of the HEWT coupons. A large scatter in the joint failure load and failure mode data was noticed for this joint test. The predominant failure modes of the joint are "Delam" and "NSF". The delamination failure mode occurred at a lower load than the net-section failure mode for the coupons. Two coupons failed in a delamination only failure mode at an average test load of 59.829 kN. Four coupons failed in a net-section only failure mode at an average test load of 69.785 kN. The six coupons that failed by either delamination or a combination of the delamination or net-section failure modes failed at a test average of 64.785 kN. The pre-test progressive failure analysis predictions of the HEWT coupon was 66.674 kN which was within 1% of the average test failure coupon failure load. If the coupons that failed by net-section failure are not included in the comparison, then the pre-test predictions were still within 3% of the average test failure load for those six coupons. Post-test analysis failure predictions were not pursued since the pre-test predictions were within 5% of the test data which was a goal of the project. Delamination between the face sheet plies were predicted for this coupon. The progression of delamination as a function of load is presented in Figure 16. Even though splice plates were not analyzed for damage, stresses in them were noticed to reach the allowable limit as the model reached failure. A future work is planned to include a PFA model for the fabric of the splice plates. Hence the PFA was capable of capturing the delamination mode of failure between the face sheet plies and not the net section failure of the splice plates.

Table 3. Test Data of HEWT Coupons.

Specimen ID	Test Failure Load (kips)	Failure Mode
CTE-300-1-HT-P-1	71.692	Delam/NSF
CTE-300-1-HT-P-2	61.239	Delam/NSF
CTE-300-1-HT-P-3	69.321	Delam/NSF
CTE-300-1-HT-P-4	57.840	Delam
CTE-300-1-HT-P-5	61.817	Delam
CTE-300-3-HT-P-1	69.686	NSF
CTE-300-3-HT-P-2*	67.595	NSF
CTE-300-3-HT-P-3	66.803	Delam/NSF
CTE-300-3-HT-P-4	70.687	NSF
CTE-300-3-HT-P-5	71.172	NSF
Average	**66.785**	

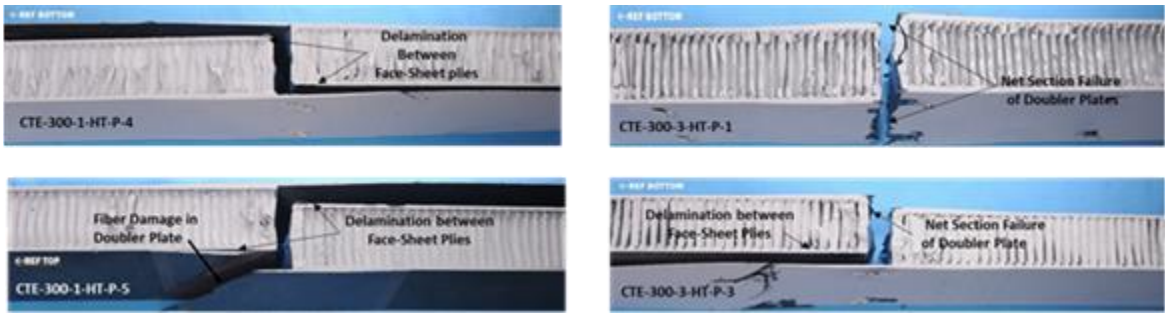

Figure 15. Typical Damage Modes in HEWT Coupons.

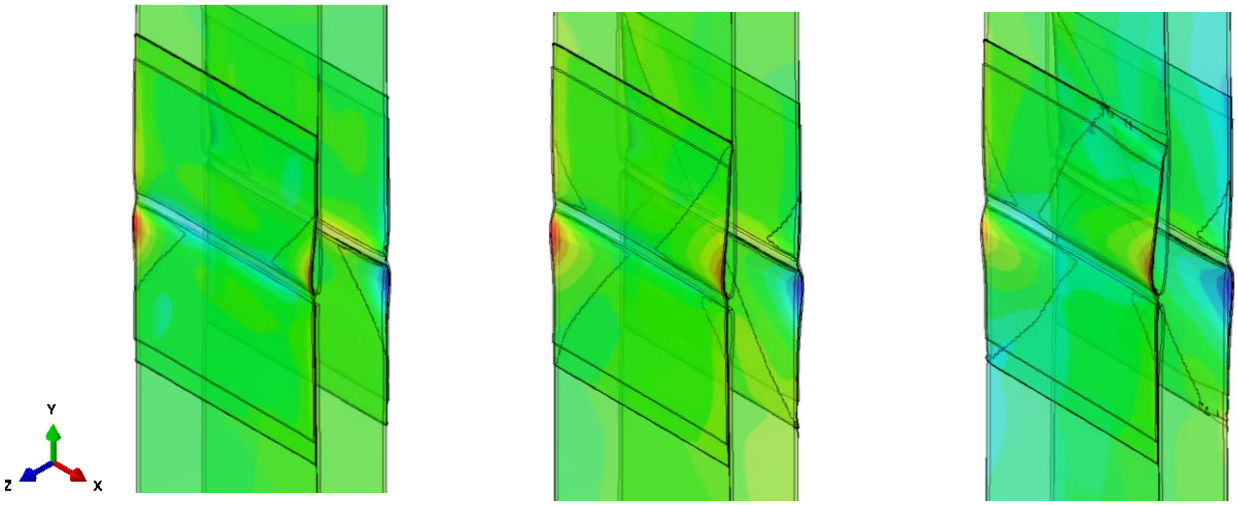

U_z Displacement Contours (At 61.39 kN)

U_z Displacement Contours (At 65.21 kN)

U_z Displacement Contours (At 66.72 kN)

Figure 16 Delamination Progression as a Function of in HEWT Model.

4. CONCLUSIONS

The NASA Composite Technology for Exploration (CTE) Project is developing and demonstrating critical composite technologies with a focus on composite bonded joints; incorporating materials, design/analysis, manufacturing, and tests that utilize NASA expertise and capabilities. The project has goals of advancing composite technologies providing lightweight structures to support future NASA exploration missions. In particular, the CTE project is demonstrating weight-saving, performance-enhancing composite bonded joint technology for Space Launch System (SLS)-scale composite hardware. Advancements from the CTE project may be incorporated as future block upgrades for SLS structural components.

This paper discussed the sub-element longitudinal bonded joint testing and analysis correlation for a generic space launch vehicle structure called the *CTE Point Design.* The *CTE Point Design* is a conical sandwich structure with a 35-degree angle consisting of eight composite sandwich segments joined together with a double lap composite joint. A description of the sub-element joint test coupon design was presented for three coupon configurations to test various critical loading conditions including axial and hoop compression and hoop tension. Longitudinal bonded joint sub-element test articles were fabricated and tested for several loading conditions to test the

capability of the joint design for the as-designed loads. The test results show that test failure loads for the composite longitudinal bonded joint design significantly exceeds the joint design loads with a 2.0 factor of safety for both pristine and impact-damage coupons. The joint tests showed repeatable test failure loads and failure mechanisms leading to joint failure. The analysis pre-test failure load predictions were +8.8 % of the average test failure load for the AEWC coupons, -3.0 % of the average test failure load for the HEWC coupons, and within 1 % of the average test coupon failure load for the HEWT coupons. Post-test analyses were performed on the AEWC coupons to improve the analysis failure load prediction to be +3.3 % of the average test failure load. The PFA also accurately predicted the dominant failure mode for each sub-element joint test. This testing and analysis provides confidence in the potential use of composite bonded joints for future launch vehicle structures.

5. REFERENCES

1. Kirsch, Michael, T. "Composite Crew Module: Primary Structure," NASA/TM-2011-217185.
2. Johnson, T. F., Sleight, D. W., and Martin, R. A., "Structures and Design Phase I Summary for the NASA Composite Cryotank Technology Demonstration Project," 54th AIAA/ASME/ASCE/AHS/ ASC Structures, Structural Dynamics, and Materials Conference, Boston, MA, April 2013.
3. Fikes, J. C., Jackson, J. R., Richardson, S. W., Thomas, A. S., and, T. O., and Miller, S. G., "Composites for Exploration Upper Stage," NASA/TM-2016-219433, December 2016.
4. Sleight, David. W., Rosario, S., Johnson, T. F., and Shular, D. A., "Composite Cryotank Technology Demonstration 5.5-Meter Diameter Pre-Test, Analysis and Test Readiness," NASA/TM-2016-219325.
5. Mann, T., Smeltzer, S., Grenoble, R. W., Mason, B. H., Rosario, S., & Fairbairn, R., "Sizing and Lifecycle Cost Analysis of an Ares V Composite Interstage", AIAA 2012-1770, 53rd AIAA/ASME/ASCE/AHS/ASC Structures, Structural Dynamics, and Materials Conference, Honolulu, HI, April 2012.
6. Sleight, D. W., Segal, K. N., Guin, W. E., McDougal, M. R., Wolfe, C. C., Johnston, M. M., and Miller, S. G., "Development of Composite Sandwich Bonded Longitudinal Joints for Space Launch Vehicle Structures", AIAA Sci-Tech 2019.
7. NX Nastran, Software Package, Ver. 10, Siemens PLM Software, Inc., Plano, TX, 2014
8. Satyanarayana, A., Bogert, P., Karayev, Z. K., Nordman, S. P., Hamid, "Influence of Finite Element Size in Residual Strength Prediction of Composite Structures," Proceedings of the 53rd AIAA/ASME/ASCE/AHS/ASC Structures, Structural Dynamics and Materials Conference, Honolulu, Hawaii, April 2012, AIAA-2012-1619.
9. Abaqus, Software Package, Ver. 6.13, Dassault Systèmes, Waltham, MA, 2013.
10. Mason, B. H., Satyanarayana, A., and Sleight, D. W., "Test and Analysis Correlation for Sandwich Composite Longitudinal Joint Specimens," AIAA Sci-Tech 2019.